

Stability analysis of MHD stagnation flow over a permeable heated rotating disk with heat generation/absorption

F. MENDIL^{*}), S. MAMACHE, F. N. BOUDA

Université de Bejaia, Faculté de Technologie, Laboratoire de Mécanique, Matériaux et Énergétique (L2ME), 06000 Bejaia, Algeria, e-mail^{}): fatsah.mendil@univ-bejaia.dz (corresponding author)*

THE STAGNATION POINT FLOW OF AN INCOMPRESSIBLE VISCOUS electrically conducting fluid impacting orthogonally on a heated rotating disk is studied with internal volumetric heat generation/absorption in the presence of a uniform magnetic field. A uniform suction or injection is applied through the surface of the disk. Appropriate similarity transformations are used to reduce the governing differential equations of the problem into a system of nonlinear ordinary differential equations and then solved numerically using the fourth-order Runge–Kutta method. In the second step, the work is oriented towards linear stability analysis by considering infinitesimally small disturbances within the boundary layer. Using normal mode decomposition in the Görtler–Hammerlin framework, the resulting eigenvalue problem is then solved numerically by means of the pseudo-spectral method using Laguerre’s polynomials. As a result, the critical conditions for the onset of thermal instability are described and discussed in detail using multiple configurations. It is found that the presence of a magnetic field and suction/injection act to increase the stability of the basic flow. However, the rotation parameter and the internal heat generation/absorption contribute significantly to destabilizing the basic flow.

Key words: stability analysis, boundary layer, rotating disk, MHD flow, heat generation/absorption.



Copyright © 2024 The Authors.

Published by IPPT PAN. This is an open access article under the Creative Commons Attribution License CC BY 4.0 (<https://creativecommons.org/licenses/by/4.0/>).

1. Introduction

RECENT RESEARCH IN THE FIELD OF ENGINEERING AND INDUSTRIAL applications has paid much attention to the study of the MHD flow over a rotating disk. Theoretical and experimental studies for the MHD flow over a rotating disk with heat transfer appear interesting in different versatile applications. Much effort on this phenomenon has been focused on a wide range of areas such as air cleaners, gas turbine rotors, medical equipment, chemical vapor deposition processes, aerodynamic engineering and thermal power generation systems.

In the rotating disk systems, the hydrodynamic flow of a rotating infinite disk was originally initiated by VON KÁRMÁN [1] who introduced the first simi-

larity transformations to convert partial differential equations into ordinary differential equations. Orthogonal forced flow was first examined by HANNAH [2]. The influence of a uniform external magnetic field on a steady flow generated by the rotating disk was examined in [3, 4]. The stagnation point flow problem has been extended in various interesting applications with different physical characteristics, where the effect of uniform suction/injection on the steady axisymmetric flow of an incompressible viscous electrically conducting fluid with heat transfer was investigated by ATTIA [5]. ARIKOGLU *et al.* [6] have introduced a semi-numerical analytical technique to analyze the effect of slip on entropy generation in magnetohydrodynamic flow over a rotating disk. The effect of a uniform vertical magnetic field on the steady boundary layer stagnation flow of an electrically conducting fluid impinging on a rotating stretching disk was investigated by TURKYILMAZOGLU *et al.* [7]. IMTIAZ *et al.* [8] have considered a sliding velocity at the fluid-solid interface to analyze the characteristics of magnetohydrodynamic flow by a rotating disk of a variable thickness. HAYAT *et al.* [9] explored the heat transfer in the presence of thermal radiation in the MHD flow of a viscous fluid through a rotating disk of variable thickness. Several studies have been carried out on the famous von Kármán problem, which is extensively studied in different fields of applications. MUSTAFA [10] extended the von Kármán problem of the infinite rotating disk where the space above the rough disk is equipped by an electrically conductive nanofluid. In the presence of a magnetic field in an electrically conductive fluid flow, viscous dissipation and Joule heating is a spontaneous and inevitable phenomenon. In this field, viscous dissipation in a nanomaterial flow by a rotating disk was studied by HAYAT *et al.* [11], they then investigated the entropy generation in magnetohydrodynamic radiative flow due to rotating disk in the presence of viscous dissipation and Joule heating [12]. Recently, RAHMAN *et al.* [13] have studied the unsteady three-dimensional magnetohydrodynamics flow of nanofluids over a decelerated rotating disk with uniform suction.

The instability that governs fluid flow is a fundamental subject of fluid mechanics in which the analysis of transitional flows to turbulence is linked to heat transfer and convective motions. These flow models have been studied by many scientists to understand the boundary layer transition processes. Advances in the stability theory and experimentation of rotating flows have been increasingly confronted with fairly complex challenges in recent decades. To the authors' knowledge, few studies concerning thermal instability are available in the literature. By highlighting reported studies on the stability analysis, the stability of three-dimensional rotating-disk flow was investigated by MALIK *et al.* [14, 15]. HUERRE and MONKEWITZ [16] examined the theory of hydrodynamic stability of spatially developing flows relating to the concepts of absolute/convective and local/global instability. LINGWOOD [17] examined the characteristics of bound-

ary layer flow over a rotating disk in an otherwise still fluid by analyzing the inviscid stability of the flow and the stability with viscous curvature, Coriolis, and streamlining effects. LEE *et al.* [18] have employed the linear stability theory to analyze the stability of 3D boundary-layer flow introduced in a rotating disk system. The impact of the magnetic field of such concepts on the fluid flow instabilities can be found in [19, 20]. Stability analysis of the stagnation point flow has been the subject of numerous scientific applications associated with industry and mechanical engineering, some studies on this topic can be seen in [21–23]. HEALEY [24] examined the relation between viscous and inviscid absolute instabilities in a boundary layer flow induced by a rotating disk. The absolute and convective instability of the von Kármán rotating disk flow with a temperature-dependent viscosity was analyzed by JASMINE and GAJJAR [25]. TURKYILMAZOGLU *et al.* [26] introduced a global view clarifying the compressible viscous modes leading in particular to absolute instability in a generalized three-dimensional von Kármán boundary layer flow due to a rotating disk. The linear behavior of an impulse disturbance on the global instability of the rotating disk boundary layer was studied in a linear and nonlinear simulation by APPELQUIST *et al.* [27]. MENDIL *et al.* [28] investigated the thermal instability of two-dimensional stagnation point flow in temperature-dependent viscosity fluid. BOUDA *et al.* [29] analyzed the effects of mass transfer on the thermal instability of a two-dimensional boundary layer stagnation point flow when thermal and concentration buoyancy forces are of opposite signs. The onset of instabilities of a two-dimensional mixed convection boundary layer flow induced by an impinging ascending flow on a heated horizontal cylinder was studied in [30]. From recent studies on the stagnation point flow, MILLER *et al.* [31] have analyzed the linear stability analysis of temperature-dependent boundary layer flow on a rotating disk. MUKHERJEE and SAHOO [32] investigated the effect of slip condition on the convective instability characteristics of the stagnation point flow over a rough rotating disk. An experimental investigation of the effect of heating on the stability of three-dimensional boundary layer flow over a rotating disk was performed by WIESCHE and HELCIG [33].

The transition from laminar to turbulent flow with heat transfer remains a large-scale open problem, of which the current paper focuses on the stability analysis of the stagnation point flow of an electrically conducting fluid, in the presence of a magnetic field, suction/injection and internal heat generation/absorption effects. Our main motivation is to extend the previous studies by analyzing the critical conditions for the onset of thermal instabilities. For this purpose, the resulting eigenvalue problem has been constituted by applying the linear stability theory based on the normal mode decomposition of Görtler–Hammerlin [34, 35], which is solved numerically by means of a pseudo-spectral collocation method using Laguerre’s polynomials. It is found that the presence

of a magnetic field and suction/injection act to increase the stability of the basic flow. However, the critical conditions for the onset of thermal instability are significantly affected by the internal heat generation/absorption parameter, and increasing this parameter decreases the stability of the basic flow.

2. Problem statement and mathematical formulation

We consider the steady incompressible MHD flow impinging on a heated permeable disk rotating about its axis with a constant angular velocity Ω^* . In the cylindrical coordinate system, the external velocity is prescribed as $\mathbf{V}_\infty^*(ar^*, 0, -2az^*)$, where a is a positive constant characterizing the velocity of the mainstream flow. Let p^* , T , u^* , v^* and w^* denote the steady state of the pressure, temperature and velocity in the r^* , θ , and z^* directions, respectively. The coordinate frame is not related to the disk rotation, and the disk is maintained at a fixed temperature T_w higher than the ambient fluid temperature T_∞ . The heat transfer process is explored subject to internal volumetric heat generation/absorption. The uniform magnetic field is applied in z^* -direction with the strength B as shown in Fig. 1.

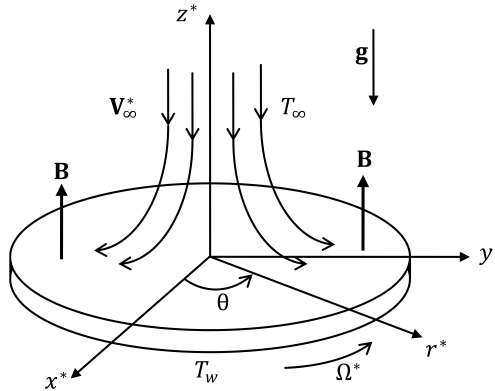


FIG. 1. Physical model for flow domain.

The physical properties of the fluid are assumed constant except the density in the buoyancy force term, which is satisfied by the Boussinesq approximation. The magnetic Reynolds number is assumed to be small so that the induced magnetic field can be neglected. In addition, there is no applied electric field and all of the Hall effect, viscous dissipation, and Joule heating are neglected. Under these assumptions, the conservation of mass, momentum, and energy equations are given in their dimensional form of temperature T and velocity \mathbf{V}^* as follows [22, 36]:

$$(2.1) \quad \nabla \cdot \mathbf{V}^* = 0,$$

$$(2.2) \quad \frac{\partial \mathbf{V}^*}{\partial t^*} + (\mathbf{V}^* \cdot \nabla) \mathbf{V}^* = -\frac{1}{\rho} \nabla p^* + \nu \nabla^2 \mathbf{V}^* - \mathbf{g} \beta (T - T_\infty) + \frac{\sigma}{\rho} (\mathbf{V}^* \wedge \mathbf{B}) \wedge \mathbf{B},$$

$$(2.3) \quad \frac{\partial T}{\partial t^*} + (\mathbf{V}^* \cdot \nabla) T = \frac{1}{\rho C_p} \{k \nabla^2 T + Q^*(T - T_\infty)\}.$$

In the above equations, stars (*) indicate dimensional quantities, t^* denotes the time, \mathbf{g} the gravitational acceleration, and Q^* is the internal volumetric heat generation/absorption. Here, ρ , ν , σ , β , C_p and k are respectively the density, kinematic viscosity, electrical conductivity, thermal expansion coefficient, specific heat, and thermal conductivity of the fluid.

The system of equations (2.1)–(2.3) is subject to the following boundary conditions, such that the radial and azimuthal velocities on the disk are subject to non-slip conditions, while the axial one is subject to the uniform suction/injection through the disk. Far from the disk, the flow tends to the external stream. Concerning the thermal conditions, the temperature at the disk is maintained at (T_w) , whereas, at the infinity, it is assumed that the temperature is equal to that of the external flow (T_∞) such as:

$$(2.4) \quad u^* = 0, \quad v^* = r^* \Omega^*, \quad w^* = w_S, \quad T = T_w \quad \text{at } z^* = 0,$$

$$(2.5) \quad u^* = ar^*, \quad v^* = 0, \quad w^* = -2az^*, \quad T = T_\infty \quad \text{as } z^* \rightarrow \infty,$$

where w_S is the velocity of suction ($w_S < 0$) or injection ($w_S > 0$) through the disk. The subscripts (w) and (∞) stand for the wall and free stream conditions. For the problem modeling, the dimensionless form of the equation system is achieved by the scale variables given below:

$$(2.6) \quad t = at^*, \quad (r, z) = \sqrt{\frac{a}{\nu}} (r^*, z^*), \quad \mathbf{V} = \sqrt{\frac{1}{\nu a}} \mathbf{V}^*, \quad \Theta = \frac{T - T}{T_w - T_\infty}, \quad p = \frac{p^*}{\rho \nu a}.$$

3. Solution of the basic flow

In order to resolve the steady basic flow, all the physical quantities are assumed to be independent of the (θ) variable since the flow is axisymmetric around the z^* -axis. Applying the scaling variables (2.6) and the boundary layer approximation, the resulting equation system becomes in its dimensionless form as follows:

$$(3.1) \quad \frac{\partial u}{\partial r} + \frac{u}{r} + \frac{\partial w}{\partial z} = 0,$$

$$(3.2) \quad u \frac{\partial u}{\partial r} - \frac{v^2}{r} + w \frac{\partial u}{\partial z} = -\frac{\partial p}{\partial r} + \frac{\partial^2 u}{\partial r^2} + \frac{1}{r} \frac{\partial u}{\partial r} - \frac{u}{r^2} + \frac{\partial^2 u}{\partial z^2} - Mu,$$

$$(3.3) \quad u \frac{\partial v}{\partial r} + \frac{uv}{r} + w \frac{\partial v}{\partial z} = \frac{\partial^2 v}{\partial r^2} + \frac{1}{r} \frac{\partial v}{\partial r} - \frac{v}{r^2} + \frac{\partial^2 v}{\partial z^2} - Mv,$$

$$(3.4) \quad u \frac{\partial w}{\partial r} + w \frac{\partial w}{\partial z} = -\frac{\partial p}{\partial z} + \frac{\partial^2 w}{\partial r^2} + \frac{1}{r} \frac{\partial w}{\partial r} + \frac{\partial^2 w}{\partial z^2} - Gr \Theta,$$

$$(3.5) \quad u \frac{\partial \Theta}{\partial r} + w \frac{\partial \Theta}{\partial z} = \frac{1}{Pr} \left(\frac{\partial^2 \Theta}{\partial r^2} + \frac{1}{r} \frac{\partial \Theta}{\partial r} + \frac{\partial^2 \Theta}{\partial z^2} \right) + Q\Theta.$$

The above equations can be reduced, after eliminating the pressure term by subtracting Eq. (3.2) from Eq. (3.4) after deriving them with respect to $(\partial/\partial r, \partial/\partial z)$, respectively. The buoyancy force term shown in Eq. (3.4) is expressed in terms of the Grashof number $Gr = (g\beta(T_w - T_\infty)\ell^3/v^2)$, where $\ell = (v/a)^{1/2}$. Here, $Pr = (v/\alpha)$ is the Prandtl number, $M = (\sigma B^2 \ell^2/\mu)$ is the magnetic parameter (the Hartmann number squared), where α and μ are respectively the thermal diffusivity and dynamic viscosity of the fluid, $Q = (Q^*/(a\rho Cp))$ is the internal heat generation/absorption parameter.

After introducing the following similarity transformation [10]:

$$(3.6) \quad u(r, z) = r f'(z), \quad v(r, z) = r h(z), \quad w(r, z) = -2f(z), \quad \Theta(r, z) = \Theta(z),$$

thanks to such a form of similarity transformation, the continuity equation (3.1), is automatically satisfied. Then, Eqs. (3.1)–(3.5) are written in terms of $f(z)$, $h(z)$ and $\Theta(z)$ leading to the following coupled nonlinear ordinary differential equations:

$$(3.7) \quad f''' + 2ff'' - f'^2 + h^2 + M(1 - f') + 1 = 0,$$

$$(3.8) \quad h'' - 2f'h + 2fh' - Mh = 0,$$

$$(3.9) \quad \Theta'' + 2Pr f\Theta' + Q\Theta = 0,$$

where the prime denotes differentiation with respect to z . Note that the system of Eqs. (3.7)–(3.9) can be compared with that one established in [5, 8, 14].

The transformed boundary conditions are given by:

$$(3.10) \quad \begin{cases} f(0) = S, f'(0) = 0, h(0) = \Omega, \Theta(0) = 1 & \text{at } z = 0, \\ f'(\infty) = 1, h(\infty) = \Theta(\infty) = 0 & \text{as } z \rightarrow \infty, \end{cases}$$

where $\Omega = (\Omega^*/a)$ denotes the dimensionless rotation parameter and $S = -(w_S/2\sqrt{va})$ is the uniform suction ($S > 0$) or the injection ($S < 0$) parameter.

At the disk, the mathematical expression of the shear stresses in the radial and tangential directions τ_r and τ_θ are defined as follows:

$$(3.11) \quad \begin{aligned} \tau_r &= \mu \left(\frac{\partial u^*}{\partial z^*} + \frac{\partial w^*}{\partial r^*} \right) \Big|_{z^*=0}, & \tau_\theta &= \mu \left(\frac{\partial v^*}{\partial z^*} + \frac{1}{r^*} \frac{\partial w^*}{\partial \theta} \right) \Big|_{z^*=0}, \\ C_f &= \frac{\sqrt{\tau_r^2 + \tau_\theta^2}}{\rho(ar)^2}. \end{aligned}$$

Using the similarity transformation (3.6), the local skin friction coefficient is given as

$$(3.12) \quad rC_f = \sqrt{f''(0)^2 + h'(0)^2}.$$

The rate of heat transfer is defined as

$$(3.13) \quad Nu = \frac{r^* q_w}{k(T_w - T_\infty)} \Big|_{z^*=0} \quad \text{with} \quad q_w = -k \frac{\partial T}{\partial z^*} \Big|_{z^*=0}.$$

In dimensionless form, the local Nusselt number can be written in the following form:

$$(3.14) \quad Nu/r = -\Theta'(0).$$

By integrating the shooting method, the coupled nonlinear ordinary differential equations (3.7)–(3.9) along with their boundary conditions (3.10) are solved numerically using the fourth-order Runge–Kutta method. In all calculations, the step size is taken as $\Delta z = 0.01$ and the process is repeated until a desired precision of 10^{-6} . However, for such a level of accuracy, the iterative process required a significant increase in calculation time. The resolution of the equations system was carried out for $\Omega = [0, 1]$, $Pr = [0.7, 7]$, $M = [0, 15]$, $S = [-1.5, 1.5]$ and $Q = [-0.4, 0.4]$, and the characteristics of the velocity and heat transfer fields obtained from these solutions are presented in Section 6.

4. Linear stability analysis

The process of linear stability analysis consists of identifying the wavenumbers and frequencies corresponding to the waves supported by the system. Most stability studies generally adopt a purely temporal or spatial instability approach. However, introducing the concepts of absolute and convective instability has revealed the limitations of relying only on spatial or temporal instability analysis. In [17, 24], the temporal theory assumes that disturbances develop over time from an initial spatial distribution. This would imply that the wave number is real and the frequency is complex. As for a spatial theory, it assumes the opposite case. Thus, the disturbances evolve in space from an initial temporal distribution. In the problem at hand, we are interested in temporal instability where the perturbations increase with time at each fixed point in space [21, 23]. To understand the destabilizing mechanisms linked to the transition to secondary flow, the work is oriented towards linear stability analysis to examine the temporal growth and spatial amplification related to the different stages of the transition to turbulence. The stability analysis then involves

imposing infinitesimally small disturbances on the mean flow so that the instantaneous quantities $\bar{q} = (\bar{u}, \bar{v}, \bar{w}, \bar{P}, \bar{\Theta})$ can be expressed as the sum of the basic-state $q = (u, v, w, p, \Theta)$ and the disturbance-state $\tilde{q} = (\tilde{u}, \tilde{v}, \tilde{w}, \tilde{p}, \tilde{\Theta})$ quantities as:

$$(4.1) \quad \bar{q}(r, \theta, z, t) = q(r, z) + \tilde{q}(r, \theta, z, t).$$

Introducing the above decompositions (4.1) into the governing equations of continuity, momentum and energy, by subtracting the base state and neglecting the nonlinear terms, i.e. $\tilde{u}(\partial\tilde{u}/\partial r)$, the mean-flow solutions are now subject to small perturbation quantities leading to:

$$(4.2) \quad \frac{\partial\tilde{u}}{\partial r} + \frac{\tilde{u}}{r} + \frac{1}{r} \frac{\partial\tilde{v}}{\partial\theta} + \frac{\partial\tilde{w}}{\partial z} = 0,$$

$$(4.3) \quad \left(\frac{\partial}{\partial t} + \frac{\partial u}{\partial r} + u \frac{\partial}{\partial r} + \frac{v}{r} \frac{\partial}{\partial\theta} + w \frac{\partial}{\partial z} - \nabla^2 + M \right) \tilde{u} - 2 \frac{v}{r} \tilde{v} + \frac{\partial u}{\partial z} \tilde{w} + \frac{\partial \tilde{p}}{\partial r} = 0,$$

$$(4.4) \quad \left(\frac{\partial v}{\partial r} + \frac{v}{r} \right) \tilde{u} + \left(\frac{\partial}{\partial t} + u \frac{\partial}{\partial r} + \frac{v}{r} \frac{\partial}{\partial\theta} + w \frac{\partial}{\partial z} + \frac{u}{r} - \nabla^2 + M \right) \tilde{v} + \frac{\partial v}{\partial z} \tilde{w} + \frac{1}{r} \frac{\partial \tilde{p}}{\partial\theta} = 0,$$

$$(4.5) \quad \left(\frac{\partial}{\partial t} + \frac{v}{r} \frac{\partial}{\partial\theta} + \frac{\partial w}{\partial z} + w \frac{\partial}{\partial z} - \nabla^2 \right) \tilde{w} + \frac{\partial \tilde{p}}{\partial z} + Gr \tilde{\Theta} = 0,$$

$$(4.6) \quad \left(\frac{\partial}{\partial t} + \frac{v}{r} \frac{\partial}{\partial\theta} + w \frac{\partial}{\partial z} - \frac{1}{Pr} \nabla^2 - Q \right) \tilde{\Theta} + \tilde{w} \frac{\partial \Theta}{\partial z} = 0,$$

where ∇^2 is the usual Laplacian operator in the cylindrical coordinates (r, θ, z) . Note that the quantities u, v, w , and Θ correspond to the basic flow functions given by expressions (2.6). The present work focuses on thermal instability, where the Grashof number Gr controls the problem stability and the corresponding Reynolds number ($Re = \Omega r^2$) near the stagnation point, where the flow remains laminar, is relatively small, i.e. $Re < Re_c$, where Re_c represents the critical Reynolds number. Consequently, the stability analysis of the preceding system (4.2)–(4.6) is now subject to a non-parallel-flow approximation, where the terms of order $(1/r^2)$ are considered. In the problem at hand, by considering non-parallel flow effects for thermal stability analysis, the linearized disturbance equations are not separable into r, θ and t as discussed by MALIK [15] and LINGWOOD [17]. In this case, the strong dependence of the basic state on the radial distance does not permit the introduction of eigenmodes in the radial direction as indicated in [23, 28–30]. The dimensionless Navier–Stokes

equations are linearized with respect to the disturbance quantities and give a set of equations that is separable in (θ) , and (t) is assumed to have the form

$$(4.7) \quad (\tilde{u}, \tilde{v}, \tilde{w}, \tilde{p}, \tilde{\Theta})(r, \theta, z, t) = (r\hat{u}, r\hat{v}, \hat{w}, \hat{p}, \hat{\Theta})(z) \exp(in\theta + \omega t),$$

where $\hat{u}, \hat{v}, \hat{w}, \hat{p}$ and $\hat{\Theta}$ are complex amplitude functions of three-dimensional small perturbation velocities, pressure, and temperature depending on z . The azimuthal wavenumber (n) is an integer quantity, and ω is the frequency of the disturbance in the rotating frame. The resulting stability equations are then linearized with respect to the decomposition (4.7), and the perturbation equations may be written as a set of ordinary differential equations in the following transformed variables:

$$(4.8) \quad 2\hat{u} + in\hat{v} + D\hat{w} = 0,$$

$$(4.9) \quad \left(D^2 + 2fD - 2f' - in h - M - \frac{n^2}{r^2} \right) \hat{u} + 2 \left(h - \frac{in}{r^2} \right) \hat{v} + f'' \hat{w} = \omega \hat{u},$$

$$(4.10) \quad \left(D^2 + 2fD - 2f' - in h - M - \frac{n^2}{r^2} \right) \hat{v} - 2 \left(h - \frac{in}{r^2} \right) \hat{u} - h' \hat{w} - \frac{in}{r^2} \hat{p} = \omega \hat{v},$$

$$(4.11) \quad \left(D^2 + 2fD + 2f' - in h - \frac{n^2}{r^2} \right) \hat{w} - D\hat{p} - Gr \hat{\Theta} = \omega \hat{w},$$

$$(4.12) \quad \left(D^2 + 2PrfD - in Pr h + Pr Q - \frac{n^2}{r^2} \right) \hat{\Theta} - Pr \Theta' \hat{w} = Pr \omega \hat{\Theta}.$$

The perturbations canceled out at the wall and away from the boundary layer as indicated in the following boundary conditions:

$$(4.13) \quad \begin{cases} \hat{u} = \hat{v} = \hat{w} = D\hat{w} = \hat{p} = \hat{\Theta} = 0 & \text{at } z = 0, \\ \hat{u} = \hat{v} = \hat{w} = \hat{p} = \hat{\Theta} = 0 & \text{as } z \rightarrow \infty, \end{cases}$$

where $D = \partial/\partial z$ is the differential operator with respect to z .

The pressure (\hat{p}) and the azimuthal velocity component (\hat{v}) can be deduced from Eq. (4.8) and (4.10) in the form:

$$(4.14) \quad \hat{v} = \frac{i}{n}(2\hat{u} + D\hat{w}),$$

$$(4.15) \quad \hat{p} = \frac{r^2}{n^2} \left[(D^2 + 2fD - 2f' - M - \omega)(2\hat{u} + D\hat{w}) - \left\{ \left(in h + \frac{n^2}{r^2} \right) D - in h' \right\} \hat{w} \right].$$

Then, we substitute Eq. (4.14) and (4.15) into the previous system (4.9)–(4.11), the number of unknowns can be obviously reduced. In addition,

this combination not only facilitates the numerical solution of the system but also minimizes the calculation time. Indeed, the final system can be simplified and rewritten as a set of three equations as the following form of an algebraic eigenvalue problem:

$$(4.16) \quad \left\{ D^2 + 2fD - 2f' - inh - M - \frac{n^2}{r^2} - \frac{4}{in} \left(h - \frac{in}{r^2} \right) \right\} \hat{u} - \frac{2}{in} \left(h - \frac{in}{r^2} \right) D\hat{w} + f''\hat{w} = \omega\hat{u},$$

$$(4.17) \quad \left\{ 2(D^2 + 2fD - 2f' - M)D + 4(f'D - f'') \right\} \hat{u} + \left\{ \left(D^2 + 2fD - inh - M - \frac{n^2}{r^2} \right) D^2 - 2f''D - inh'' - \frac{n^2}{r^2} \left(D^2 + 2fD + 2f' - inh - \frac{n^2}{r^2} \right) \right\} \hat{w} + \frac{n^2}{r^2} Gr \hat{\Theta} = \omega \left\{ 2D\hat{u} + \left(D^2 - \frac{n^2}{r^2} \right) \hat{w} \right\},$$

$$(4.18) \quad \left\{ D^2 + Pr(2fD - inh + Q) - \frac{n^2}{r^2} \right\} \hat{\Theta} - Pr \Theta' \hat{w} = Pr \omega \hat{\Theta},$$

with the following boundary conditions

$$(4.19) \quad \begin{cases} \hat{u} = \hat{w} = D\hat{w} = \hat{\Theta} = 0 & \text{at } z = 0, \\ \hat{u} = \hat{w} = D\hat{w} = \hat{\Theta} = 0 & \text{as } z \rightarrow \infty. \end{cases}$$

The numerical resolution of this system requires the determination of the eigenvalue ω and the corresponding eigenfunctions \hat{u} , \hat{w} and $\hat{\Theta}$ as functions of the spanwise wavenumber n . It is well known that when $\omega < 0$, the disturbances are reduced over time and the stationary solution remains linearly stable. However, when $\omega > 0$, the disturbances grow significantly with time and the flow becomes linearly unstable. At the marginality ($\omega = 0$), it is only for certain typical values of the Grashof number Gr that the above system can have a non-trivial solution for given value of n , r , Pr , Ω , Q , S and M .

5. Numerical approach to stability analysis

Stability analysis is examined by solving the generalized eigenvalue problem by means of a pseudo spectral method based on the expansion of Laguerre's polynomials $L_n(z)$. It relies on the approximation of the exact solution by polynomials. Consequently, in contrast to other methods such as the finite differences

or the finite elements, it can achieve an infinite degree of accuracy. This method is widely used in various physical configurations to approximate the boundary layer problems so that the collocation nodes z_j ($j = 1, \dots, N$) are selected to be the roots of the Laguerre polynomial of degree N . By truncating the expansion to a finite number N of terms, an approximation of the functions \hat{u} , \hat{w} and $\hat{\Theta}$ noted \hat{u}_N , \hat{w}_N and $\hat{\Theta}_N$ is given in the form $\Gamma_N(z) = \exp(-z)$, with Γ_N being a polynomial of degree at most N forced to fulfill the linear system at collocation nodes which are selected to be the zeroes of $L_n(z)$. For more details, the numerical approach has been implemented in [37]. The most important feature of this method is the exponential convergence (the error decreases exponentially), which allows high precision with a modest number of collocation points. However, the use of Laguerre's polynomials is motivated by the distribution of their zeros, i.e. the first zeros are close to each other, and this distribution is perfectly suited to describe regions of strong gradients such as the boundary layer problems. An approach of the three-dimensional complex amplitude functions is given as an approximation in the form $\hat{\phi}_N(\hat{u}_N, \hat{w}_N, \hat{\theta}_N)$ defined as being [22]:

$$(5.1) \quad \hat{\phi}_N(z) = e^{-z} \sum_{j=1}^N \frac{z L_N(z)}{z_j(z - z_j) L'_N(z_j)} \phi_N(z_j).$$

The procedure gives rise to an algebraic eigenvalue problem expressed in terms of discretized square ($3 \times N, 3 \times N$) matrices **A** and **B**:

$$(5.2) \quad \mathbf{A}(r, n, Pr, \Omega, Gr, Q, S, M) \Phi_N = \omega \mathbf{B}(r, Pr, n) \Phi_N.$$

The system of equations (4.16)–(4.18) presents the governing perturbation equations as an eigenvalue problem of the form $(\mathbf{A} - \omega \mathbf{B}) \Phi_N = 0$, where Φ_N is the vector of eigenfunctions, and the quantities **A** and **B** are square matrices containing the following non-zero coefficients terms:

$$\begin{aligned} A_{11} &= D^2 + 2(f - 1)D + \left\{ 1 - 2f - 2f' - inh - \frac{n^2}{r^2} - \frac{4}{in} \left(h - \frac{in}{r^2} \right) - M \right\} I, \\ A_{12} &= -\frac{2}{in} \left(h - \frac{in}{r^2} \right) D + \left\{ \frac{2}{in} \left(h - \frac{in}{r^2} \right) + f'' \right\} I, \\ A_{21} &= 2D^3 + 2(2f - 3)D^2 + (6 - 8f - 2M)D + (-2 + 4f + 2M - 4f'')I, \\ A_{22} &= D^4 + 2(f - 2)D^3 + \left(6 - 6f - inh - 2\frac{n^2}{r^2} - M \right) D^2 \\ &\quad + \left\{ -4 + 2 \left(3 - \frac{n^2}{r^2} \right) f + 2inh - 2f'' + 4\frac{n^2}{r^2} + 2M \right\} D \\ &\quad + \left\{ 1 - 2f + \left(\frac{n^2}{r^2} - 1 \right) inh + \frac{n^2}{r^2} \left(2f - 2f' - 2 + \frac{n^2}{r^2} \right) + 2f'' + inh'' - M \right\} I, \end{aligned}$$

$$\begin{aligned}
 A_{23} &= -\frac{n^2}{r^2} Gr I, & A_{32} &= -Pr \Theta' I, \\
 A_{33} &= D^2 + (2Pr f - 2)D + \left(1 - 2f Pr - in Pr h + Q Pr - \frac{n^2}{r^2}\right) I, \\
 B_{11} &= I, & B_{21} &= 2(D - I), \\
 B_{22} &= D^2 - 2D + \left\{1 - \left(\frac{n}{r}\right)^2\right\} I, & B_{33} &= Pr I.
 \end{aligned}$$

The problem (5.2) is posed as a linear generalized eigenvalue problem where Φ_N denotes the expansion coefficients vector. To obtain a nontrivial solution through all the calculations, the matrix $(\mathbf{A} - \omega \mathbf{B})$ must be singular or equivalently its determinant should vanish. This enables us to calculate the ω spectrum for any combination of $r, n, Pr, \Omega, S, Q, Gr$ and M parameters. The basic flow is then temporally unstable or stable whether there exists to at least one positive eigenvalue or not. The instability occurs only above some level of heating given by the lowest value of Gr obtained by varying the wavenumber n , which cancels $\det(\mathbf{A})$ at marginality. Neutral curves ($\omega = 0$) are generated using Newton's method and the iteration process is repeated until $|\det(\mathbf{A})|$ vanishes within the assumed tolerance $|\det(\mathbf{A})| \leq 10^{-6}$.

6. Results and discussion

6.1. Basic flow

Based on the numerical procedure described in the previous section, the reported results are obtained by varying the involved dimensionless variables such as the radial coordinate (r) (or radial distance), rotation parameter (Ω), Prandtl number (Pr), Hartmann number (M), suction/injection parameter (S) and internal heat generation/absorption parameter (Q). Thereafter, great attention is paid to analyzing the impact of the magnetic field, suction/injection and internal heat generation/absorption on the critical conditions for the appearance of thermal instability. Before determining the critical conditions of the onset of instability, the basic flow must be examined at the beginning since its solutions (f, h, Θ) appear as unknown terms in the generalized algebraic eigenvalue problem (5.2). Before performing the calculations for the stability analysis, we make a comparison of ours results concerning basic flow with those given in [38, 39] as shown in Table 1. Without magnetic field and suction/injection parameters ($M = S = 0$) taken into account in the present study, for the given values of Ω , the comparison shows a very high level of concordance. The numerical values of the local Nusselt number (Nu/r) are presented in Table 2, showing that the local Nusselt number increases with the increase of each parameter except Q , which presents an opposite behavior.

TABLE 1. Initial values of f'' and h' for various values of Ω when $M = S = 0$.

$f''(0)$			
Ω	Present work	HEYDARI [38]	SARKAR [39]
0	1.311938	1.311958	1.31194
1	1.573923	1.573930	1.57392
2	2.295649	2.295639	2.29564
$-h'(0)$			
1	1.1100	1.110020	1.11000

TABLE 2. Initial values of $-\Theta'(0)$ for various values of Ω , Pr , M , S and Q .

Ω	Pr	M	S	Q	$-\Theta'(0)$
0	0.7	0	0	0	0.6654
0.5					0.6696
1	0.7				0.6817
	7				1.5458
		1			1.6447
		3			1.7543
		5			1.8287
			-0.2		0.4967
			0.05		2.1717
			0.2		3.7222
				-0.4	1.8404
				0.1	1.7324
				0.4	1.6657

Figure 2 shows the resulting mean-flow profiles for a range of S and M values when $\Omega = 0.3$. Figure 2(a) presents the influence of the uniform suction/injection through the disk on the radial velocity profile $f'(z)$ with $\Omega = 0.3$ and $M = 3$. The graphs reveal that increasing S leads to a significant growth in $f'(z)$. Compared with $S = 0$, the radial velocity field is more significant in the case of suction velocity ($S > 0$). From Fig. 2(b), it appears that the impact of the magnetic field becomes important as it increases, showing a significant increase in radial velocity fields and a progressive reduction in the boundary-layer thickness.

Figure 3 depicts the change in the azimuthal velocity field for varying values of suction/injection parameter, the Hartmann number and the rotation parameter. It is shown from this figure, that the velocity field and the related boundary-layer thickness are reduced with increasing S . Here, $M \neq 0$ yields to the hydromagnetic flow situation and $M = 0$ represents the hydrodynamic case. Figure 3(b)

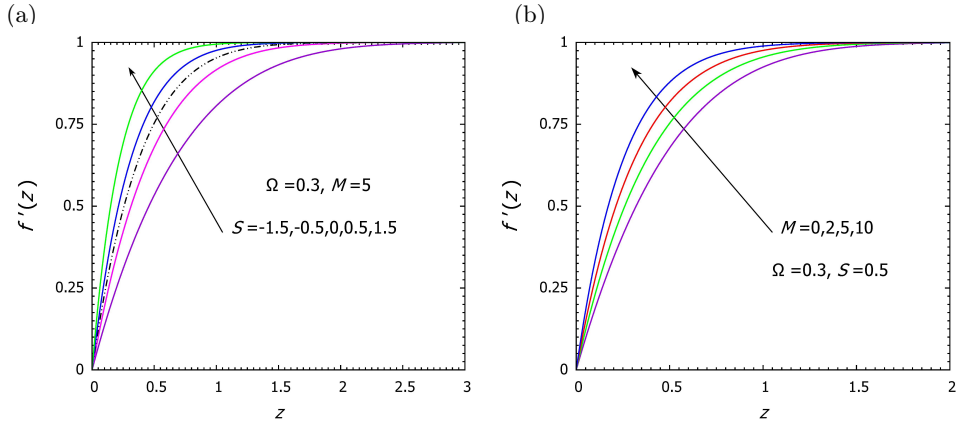


FIG. 2. Variation of $f'(z)$ for different values of: (a) suction/injection parameter S , (b) Hartmann number M .

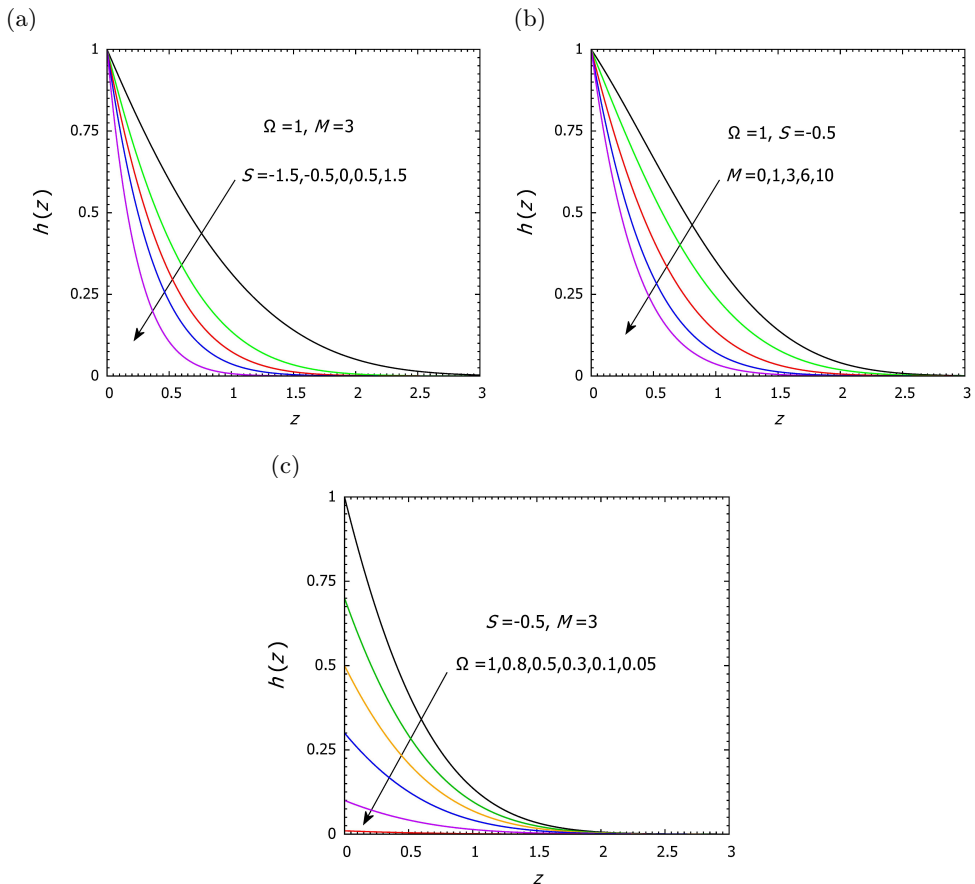


FIG. 3. Variation of $h(z)$ for different values of: (a) suction/injection parameter S , (b) Hartmann number M , (c) rotation parameter Ω .

shows the behavior of the azimuthal velocity by the varying Hartmann number M . The results show that the azimuthal velocity decays for higher M . In Fig. 3(b), at a specified value of $S = -0.5$ and $M = 3$, it is noted that the azimuthal velocity decreases with increasing Ω .

Figure 4 displays the dimensionless temperature profile for several values of the heat generation/absorption parameter and the Prandtl number in the presence of a magnetic field. Figure 4(a) indicates that an increase in Q shows a notable improvement in the temperature field's distribution as well as in the associated thermal boundary layer thickness. Figure 4(b) presents the variation in the temperature field as a function of the Prandtl number. It has been noticed that the temperature profile decreases with increasing Pr , meaning that the variations in Pr have the tendency to reduce the thermal boundary-layer thickness as Pr increases.

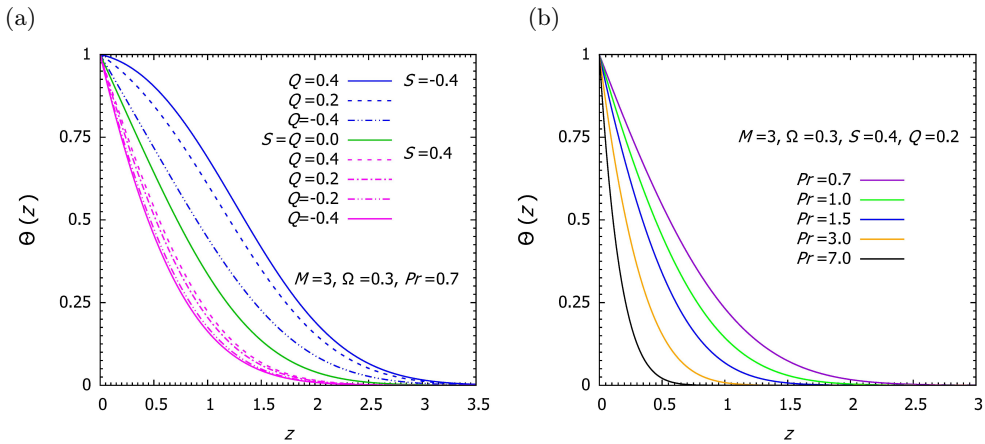


FIG. 4. Variation of $\Theta(z)$ for different values of: (a) internal heat generation/absorption Q , (b) Prandtl number Pr .

The impact of the suction/injection effect (S) on the skin friction coefficient with respect to M is presented in Fig. 5(a). It is noted that the local skin friction coefficient (rC_f) increases with increasing S and shows an increasing behavior for the larger Hartmann number M . The ultimate goal of Fig. 5(b) is to provide a unified view of the heat transfer rate through the disk surface. At first sight, the obtained results indicate that the behavior of the local Nusselt number (Nu/r) seems identical whatever the given values of internal heat generation/absorption parameter. Taking into account the injection effect ($S < 0$) for the prescribed value of the Prandtl number ($Pr = 7$), the heat transfer rate increases for a larger value of M . This shows that the efficiency of heat transfer to the disk surface decreases with increasing (Q). In the presence of the magnetic field, we can also confirm that the thermal boundary layer thickness is

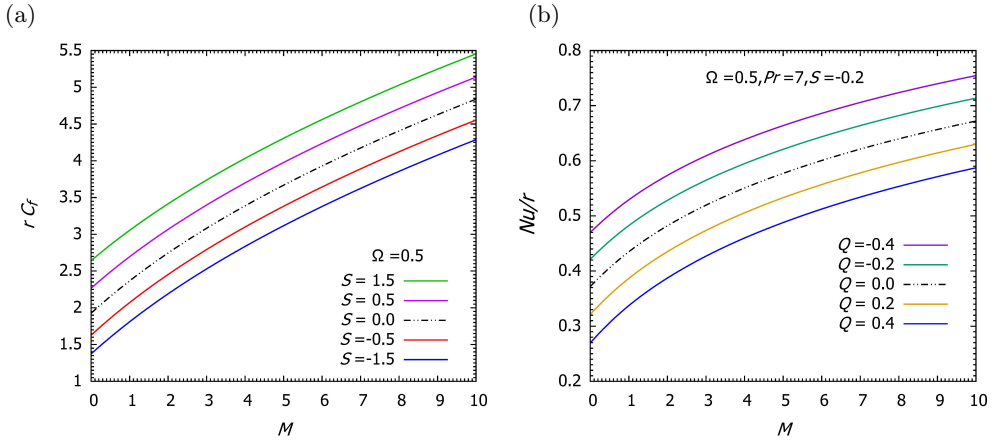


FIG. 5. Variation of local skin friction coefficient and Nusselt number with respect to M for different values of: (a) section/injection parameter S , (b) internal heat generation/absorption Q .

expanding when heat generation/absorption is allowed as shown previously in Fig. 4(a). The observations show that the heat absorption effect ($Q < 0$) has a marked impact compared to that of the heat generation effect ($Q > 0$) which has less influence on the heat transfer rate. On the other hand, the growth in the Nusselt number with internal heat generation/absorption in the presence of a magnetic field is due to the intensification of the generated vortices, which effectively enhances the convective heat transfer through the disk surface.

6.2. Stability analysis

In order to determine the critical conditions for the onset of the thermal instability that correspond to the critical Grashof number Gr_c , the numerical simulations are carried out for various combinations of the control parameters, such as Ω , Pr , Q , M and S . In all cases, the stability of the flow is examined by plotting neutral curves in the (n, Gr) plan. Furthermore, each illustrated neutral stability curve contains an unstable region located above the curve, and a stable one located below it. Our discussions focus on the critical Grashof number Gr_c , which presents the critical threshold of the transition to turbulence. With sufficiently accurate computations, the stability results confirm that the critical conditions for the onset of instability are significantly affected by the presence of a magnetic field, internal heat generation/absorption, suction/injection velocities and rotation parameters. Returning to the basics of the subject exposed in such conditions, the results show that the effect of suction/injection is similar to that of the magnetic field and that the basic flow becomes more stable as both parameters increase.

The generalized algebraic eigenvalue problem (5.2) has been solved numerically using a pseudo-spectral method based on the expansion of Laguerre’s polynomials. For satisfactory convergence, the effect of the level of truncation N was taken into account on the critical conditions for the onset of instability, which is given by the lowest value of Gr . Convergence criteria are based on the difference between iterative values of the critical Grashof number $|Gr_c^{i+1} - Gr_c^i|$. When the difference reaches 10^{-4} , i.e. $|\Delta Gr_c| < 10^{-4}$, the solution is assumed to have converged and the iterative process is terminated.

Figure 6 shows the effect of the number of collocation nodes N on the critical Grashof number error. We can see that the accuracy of the numerical scheme can be improved by increasing the number of collocation nodes. In addition, the plots reveal that the number of required polynomials increases by increasing the Hartmann number M . This is in agreement with the fact that an increase in the Hartmann number M reduces the thickness of the dynamic boundary layer; which requires a larger number of terms in order to avoid spurious nodes and preserve the prescribed precision.

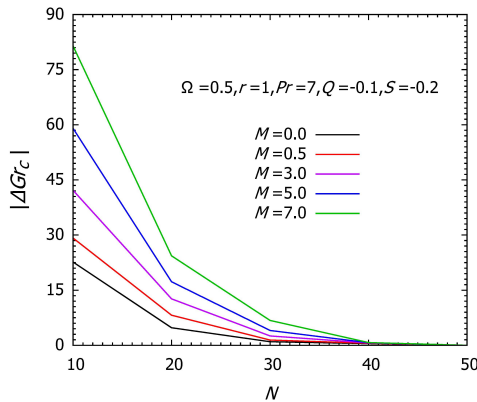


FIG. 6. Influence of the number of collocation nodes N on the critical Grashof number error.

The sequence of neutral stability curves illustrated in Fig. 7 presents an overview of the stability properties of the basic flow for different values of Ω , M , Q and S , respectively. Figure 7(a) shows that the rotation parameter Ω causes a significant change in the flow stability, which can induce strong disturbances even at low values of the rotation parameter. One can observe that the critical Grashof Gr_c decreases steadily with increasing Ω . In the (n, Gr) plane, the results presented so far show that Ω acts to destabilize the base flow, but it has nevertheless enabled us to locate the region of the growth of the most unstable modes. Figure 7(b) shows the critical Grashof numbers for different values of the Hartmann number, a regular stabilization effect is observed by increasing M ,

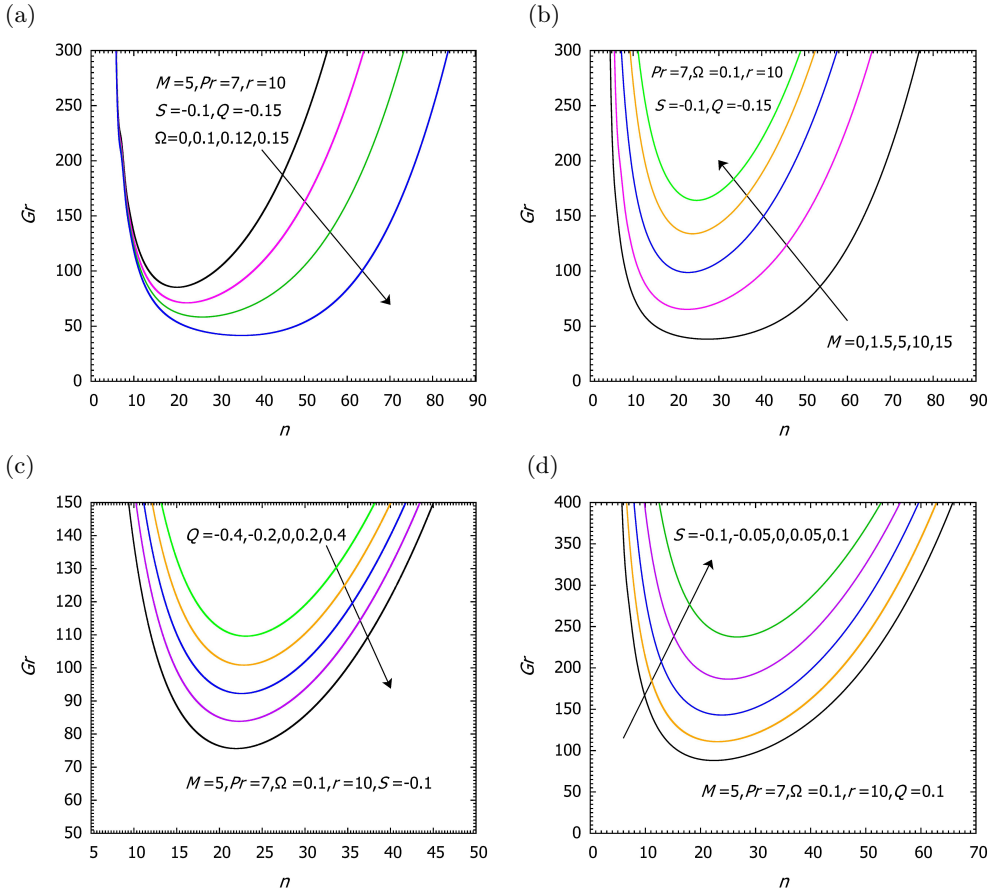


FIG. 7. Marginal stability curves for different values of: (a) rotation parameter Ω , (b) Hartmann number M , (c) internal heat generation/absorption Q , (d) suction/injection parameter S .

which leads to a significant attenuation of the instability region. This means that when the magnetic field becomes stronger, the induced Lorentz force acts to retard the transition of the basic flow [22]. The evolution of the disturbances with respect to the heat generation/absorption effect can be clarified in Fig. 7(c). The plots indicate that the flow seems more stable in the case of the absorption effect ($Q < 0$) and only when it is relatively weak, and that the heat generation ($Q > 0$) constitutes a destabilizing factor compared to $Q = 0$. Consequently, the increase in both parameters is followed by an amplification of the instability region.

Figure 7(d) presents the influence of the suction/injection velocities on the critical conditions for the appearance of instability. The results show that increasing the suction or injection velocity leads to a rapid increase in Gr_c . The plots show that the instability region in the (n, Gr) plan is contained in that

corresponding to a smaller value of suction or injection parameters. In fact, it is showed that the stability of the basic flow increases with the rise of both suction and injection parameters.

As shown in above figures, the transition to secondary flow with the parameters Ω , M , Q and S occurs at a critical Grashof number greater than the critical value of classical Hiemenz flow [40]. Specifically, the region of instability in the (n, Gr) plane, is contained in that corresponding to greater values of both the rotation parameter Ω and internal heat generation/absorption parameter Q . Furthermore, the stability region is amplified by increasing the Hartmann number M and the suction/injection parameter (S). Figure 8 shows the critical Grashof number versus the Prandtl number for several values of the Hartmann number ($M = 1, 3, 5$ and 7). When $Gr > Gr_c$, a regular destabilization effect is observed if Gr increases, but this effect is reversed when $Gr < Gr_c$ as confirmed previously in Fig. 7. The plots in Fig. 8 reveal that Gr_c increases rapidly when $Pr \rightarrow 0$, indicating that even a slight variation in Pr generates a significant variation in Gr_c . However, the Gr_c decreases rapidly when $Pr \rightarrow \infty$, leading to a significant expansion of the instability region. Physically, with the small Prandtl values, thermal disturbances tend to dissipate rapidly, and the most unstable mode remains insensitive to variations in the critical Grashof number. In this case, a higher thermal gradient is required to destabilize the basic flow. In addition, for the higher Prandtl numbers, small perturbations dissipate more slightly (decrease in Gr_c), making the equilibrium less stable.

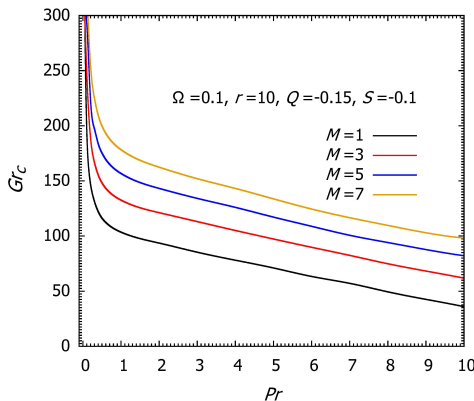


FIG. 8. Variation in critical Grashof numbers Gr_c as function of Prandtl number Pr .

The achievement for the least stable and the most unstable branches is illustrated in Fig. 9(a-c), displaying the temporal growth rate ω with respect to the wavenumber n , by varying M , Q and S . An asymptotic behavior of the critical conditions of the onset of instability seems to be confirmed in the above observations as shown previously in Fig. 7. Note that the stable region corresponds

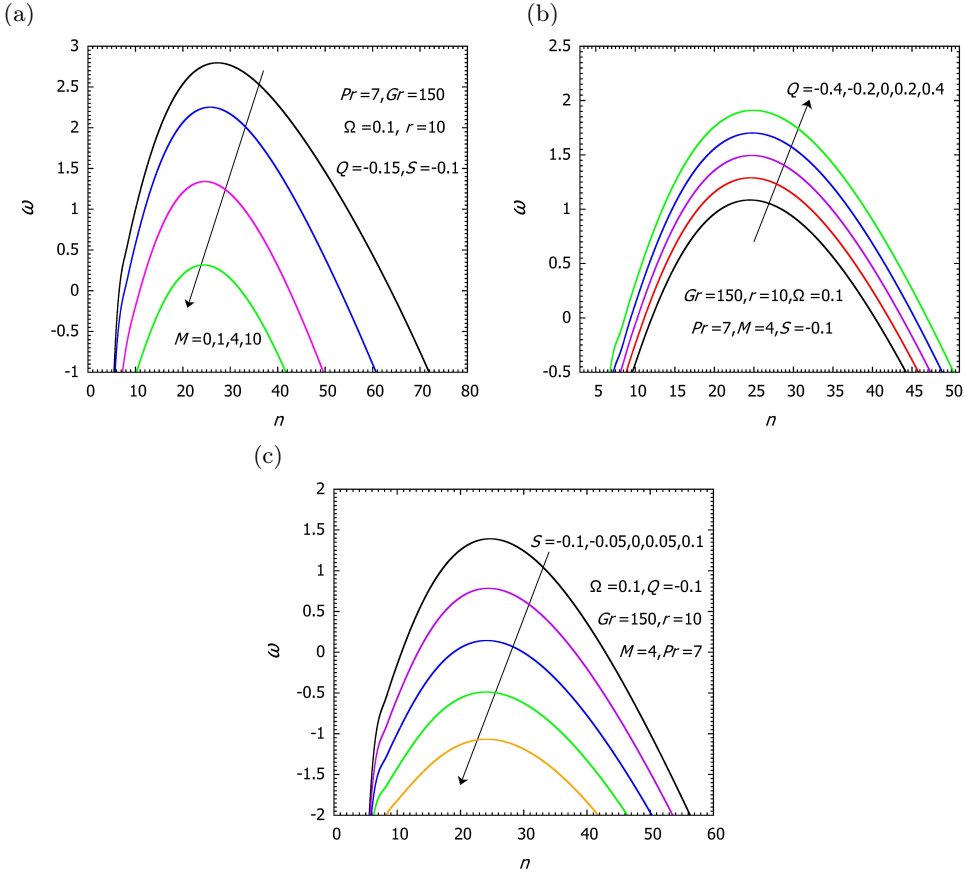


FIG. 9. Temporal growth rate as a function of wavenumber (n) for different values of: (a) Hartmann number M , (b) internal heat generation/absorption Q , (c) suction/injection parameter S .

to negative values of the temporal growth rate ($\omega < 0$), whereas, the unstable region corresponds to positive values ($\omega > 0$). The above observations show that the Hartmann number M , and the suction/injection parameter S have a significant effect on the stability of the basic flow, this means that an increase in M and S acts to retard the transition to secondary flow, and hence to reduce the thermal instability (stabilization effect). However, the increase in the magnitude of the heat generation/absorption parameter Q decreases its stability.

7. Conclusions

In this work, a linear stability analysis of a mixed convection boundary layer flow, induced by an impinging vertical descending external flow over a permeable heated rotating disk was realized. The eigenvalue problem governing the

stability process has been constituted by applying the linear stability theory which is solved numerically by means of a pseudo spectral method using Laguerre's polynomials. From the computations and the above discussions, the main results of the stability analysis can be expressed at the following findings; (i) the skin friction coefficient enhances for a larger suction/injection parameter, while the Nusselt number shows an opposite behavior with the increasing heat generation/absorption parameter. (ii) The critical Grashof number decays by increasing the rotation parameter and the heat generation/absorption effect, leading to the expansion of the instability region. However, the flow becomes more stable by increasing the suction/injection effect and the Hartmann number. (iii) The Prandtl number shows similar behavior on the stability of the flow as noted in the literature for plane and curved walls, i.e., its influence is less significant for high values. Whereas, for a very low Prandtl number, the critical Grashof number rises very rapidly even for small variations in the Prandtl number, indicating that the Prandtl number significantly affects the instability threshold. (iv) A significant decrease of the temporal growth rate of the most unstable mode and of the least stable mode with the increasing suction/injection parameter and the Hartmann number.

As a perspective, the present work can be extended to cover the modes owing to modes of absolute instability.

Conflict of interest

The authors declare that they have no conflict of interest.

References

1. T. VON KÁRMÁN, *Über laminare und turbulente Reibung [About laminar and turbulent flow]*, ZAMM – Journal of Applied Mathematics and Mechanics/Zeitschrift für Angewandte Mathematik und Mechanik, **1**, 4, 233–252, 1921, doi: 10.1002/zamm.19210010401.
2. D.M. HANNAH, *Forced flow against a rotating disc*, Reports Memoranda Aeronautical Research Council, London, **2772**, 1947.
3. E.M. SPARROW, R.D. CESS, *Magnetohydrodynamic flow and heat transfer about a rotating disk*, The Journal of Applied Mechanics, **29**, 1, 181–187, 1962, doi: 10.1115/1.3636454.
4. P.D. ARIEL, *On Computation of MHD Flow Near a Rotating Disk*, ZAMM – Journal of Applied Mathematics and Mechanics/Zeitschrift für Angewandte Mathematik und Mechanik, **82**, 4, 235–246, 2002, doi: 10.1002/1521-4001(200204)82:4<235::AID-ZAMM235>3.0.CO;2-L.
5. H.A. ATTIA, *Homann magnetic flow and heat transfer with uniform suction or injection*, Canadian Journal of Physics, **81**, 10, 1223–1230, 2003, doi: 10.1139/p03-061.
6. A. ARIKOGLU, I. OZKOL, G. KOMURGOZ, *Effect of slip on entropy generation in a single rotating disk in MHD flow*, Applied Energy, **85**, 12, 1225–1236, 2008, doi: 10.1016/j.apenergy.2008.03.004.

7. M. TURKYILMAZOGLU, *Three dimensional MHD stagnation flow due to a stretchable rotating disk*, International Journal of Heat and Mass Transfer, **55**, 23, 6959–6965, 2012, doi: 10.1016/j.ijheatmasstransfer.2012.05.089.
8. M. IMTIAZ, T. HAYAT, A. ALSAEDI, S. ASGHAR, *Slip flow by a variable thickness rotating disk subject to magnetohydrodynamics*, Results in Physics, **7**, 503–509, 2017, doi: 10.1016/j.rinp.2016.12.021.
9. T. HAYAT, S. QAYYUM, M. IMTIAZ, A. ALSAEDI, *Radiative flow due to stretchable rotating disk with variable thickness*, Results in Physics, **7**, 156–165, 2017, doi: 10.1016/j.rinp.2016.12.010.
10. M. MUSTAFA, *MHD nanofluid flow over a rotating disk with partial slip effects: Buongiorno model*, International Journal of Heat and Mass Transfer, **108**, 1910–1916, 2017, doi: 10.1016/j.ijheatmasstransfer.2017.01.064.
11. T. HAYAT, M.I. KHAN, A. ALSAEDI, M.I. KHAN, *Joule heating and viscous dissipation in flow of nanomaterial by a rotating disk*, International Communication in Heat and Mass Transfer, **89**, 190–197, 2017, doi: 10.1016/j.icheatmasstransfer.2017.10.017.
12. T. HAYAT, S. QAYYUM, M.I. KHAN, A. ALSAEDI, *Entropy generation in magnetohydrodynamic radiative flow due to rotating disk in presence of viscous dissipation and Joule heating*, Physics of Fluids, **30**, 1, 017101, 2018, doi: 10.1063/1.5009611.
13. M. RAHMAN, F. SHARIF, M. TURKYILMAZOGLU, M.S. SIDDIQUI, *Unsteady three-dimensional magnetohydrodynamics flow of nanofluids over a decelerated rotating disk with uniform suction*, Pramana Journal of Physics, **96**, 4, 170, 2022, doi: 10.1007/s12043-022-02404-0.
14. M.R. MALIK, S.P. WILKINSON, S.A. ORSZAG, *Instability and transition in rotating disk flow*, AIAA Journal, **19**, 9, 1131–1138, 1981, doi: 10.2514/3.7849.
15. M.R. MALIK, *The neutral curve for stationary disturbances in rotating-disk flow*, Journal of Fluid Mechanics, **164**, 275–287, 1986, doi: 10.1017/S0022112086002550.
16. P. HUERRE, P.A. MONKEWITZ, *Local and global instabilities in spatially developing flows*, Annual Review of Fluid Mechanics, **22**, 1, 473–537, 1990, doi: 10.1146/annurev.fl.22.010190.002353.
17. R.J. LINGWOOD, *Absolute instability of the boundary layer on a rotating disk*, Journal of Fluid Mechanics, **299**, 17–33, 1995, doi: 10.1017/S0022112095003405.
18. Y.Y. LEE, Y.K. HWANG, K.W. LEE, *The flow instability over the infinite rotating disk*, Journal of Mechanical Science and Technology, **17**, 9, 1388–1396, 2003.
19. M. TURKYILMAZOGLU, *Heat and mass transfer on the mhd fluid flow due to a porous rotating disk with hall current and variable properties*, Journal of Heat Transfer, **133**, 2, 021701 (6), 2011, doi: 10.1115/1.4002634.
20. M. TURKYILMAZOGLU, *MHD fluid flow and heat transfer due to a stretching rotating disk*, International Journal of Thermal Science, **51**, 195–201, 2012, doi: 10.1016/j.ijthermalsci.2011.08.016.
21. M. AMAOUCHE, D. BOUKARI, *Influence of thermal convection on non-orthogonal stagnation point flow*, International Journal of Thermal Science, **42**, 3, 303–310, 2003, doi: 10.1016/S1290-0729(02)00031-5.

22. M. AMAOUCHE, F.N. BOUDA, H. SADAT, *The onset of thermal instability of a two-dimensional hydromagnetic stagnation point flow*, International Journal of Heat and Mass Transfer, **48**, 21, 4435–4445, 2005, doi: 10.1016/j.ijheatmasstransfer.2005.05.003.
23. M. AMAOUCHE, F. NAÏT-BOUDA, H. SADAT, *Oblique axisymmetric stagnation flows in magnetohydrodynamics*, Physics of Fluids, **19**, 11, 114106, 2007, doi: 10.1063/1.2804957.
24. J.J. HEALEY, *On the relation between the viscous and inviscid absolute instabilities of the rotating-disk boundary layer*, Journal of Fluid Mechanics, **511**, 179–199, 2004, doi: 10.1017/S0022112004009565.
25. H.A. JASMINE, J.S.B. GAJJAR, *Absolute and convective instabilities in the incompressible boundary layer on a rotating disk with temperature-dependent viscosity*, International Journal of Heat and Mass Transfer, **48**, 5, 1022–1037, 2005, doi: 10.1016/j.ijheatmasstransfer.2004.07.036.
26. M. TURKYILMAZOGLU, N. UYGUN, *Compressible modes of the rotating-disk boundary-layer flow leading to absolute instability*, Studies in Applied Mathematics, **115**, 1, 120, 2005, doi: 10.1111/j.1467-9590.2005.01549.
27. E. APPELQUIST, P. SCHLATTER, P.H. ALFREDSSON, R.J. LINGWOOD, *Investigation of the global instability of the rotating-disk boundary layer*, Procedia IUTAM, **14**, 321–328, 2015, doi: 10.1016/j.piutam.2015.03.054.
28. F. MENDIL, F. N. BOUDA, D. SADAoui, *Effect of temperature dependent viscosity on the thermal instability of two-dimensional stagnation point flow*, Mechanics & Industry, **16**, 506, 2015, doi: 10.1051/meca/2015031.
29. F.N. BOUDA, F. MENDIL, D. SADAoui, K. MANSOURI, M. AMAOUCHE, *Instability of opposing double diffusive convection in 2D boundary layer stagnation point flow*, International Journal of Thermal Science, **98**, 192–201, 2015, doi: 10.1016/j.ijthermalsci.2015.07.014.
30. S. MOULOUD, F. NAÏT-BOUDA, D. SADAoui, F. MENDIL, *The onset of instabilities in mixed convection boundary layer flow over a heated horizontal circular cylinder*, Journal of Thermal Science and Engineering Applications, **11**, 051002, 2019, doi: 10.1115/1.4042586.
31. R. MILLER, P. GRIFFITHS, Z. HUSSAIN, S.J. GARRETT, *On the stability of a heated rotating-disk boundary layer in a temperature-dependent viscosity fluid*, Physics of Fluids, **32**, 024105, 2020, doi: 10.1063/1.5129220.
32. D. MUKHERJEE, B. SAHOO, *The effect of slip on the convective instability characteristics of the stagnation point flow over a rough rotating disk*, Kyungpook Mathematical Journal, **61**, 831–843, 2021, doi: 10.5666/KMJ.2021.61.4.831.
33. S. WIESCHE, C. HELCIG, *Effect of heating on the stability of the three-dimensional boundary layer flow over a rotating disk*, E3S Web of Conferences **345**, 02007, 2022, doi: 10.1051/e3sconf/202234502007.
34. H. GÖRTLER, *Dreidimensionale Instabilität der ebenen Staupunktströmung gegenüber wirbelartigen Strömungen [Two-dimensional instability of the same stall-point string opposite the spinning string]*, [in:] 50 Jahre Grenzschichtforschung, Vieweg und Sohn, pp. 304–314, 1955, doi: 10.1007/978-3-663-20219-6_30.
35. G. HÄMMERLIN, *Zur Instabilitäts theorie der ebenen Staupunktströmung [Towards the theory of instability of the equal staunch point strength]*, in: H. Görtler, W. Tollmein (Eds.),

50 Jahre Grenzschichtforschung, Vieweg und Sohn, pp. 315–327, 1955, doi: 10.1007/978-3-663-20219-6_31.

36. T. HAYAT, S. QAYYUM, M.I. KHAN, A. ALSAEDI, *Entropy generation in magnetohydrodynamic radiative flow due to rotating disk in presence of viscous dissipation and Joule heating*, Physics of Fluids, **30**, 1, 017101, 2018, doi: 10.1063/1.5009611.
37. C. BERNARDI, Y. MADAY, *Spectral methods, Handbook of Numerical Analysis, in Techniques of Scientific Computing (Part 2)*, Elsevier, Vol. 5, pp. 209–485, 1997, doi: 10.1016/S1570-8659(97)80003-8.
38. M. HEYDARI, G.B. LOGHMANI, M.M. RASHIDI, S.M. HOSSEINI, *A numerical study for off-centered stagnation flow towards a rotating disc*, Propulsion and Power Research, **4**, 3, 169–178, 2015, doi: 10.1016/j.jprr.2015.07.004.
39. S. SARKAR, B. SAHOO, *Oblique stagnation flow towards a rotating disc*, European Journal of Mechanics – B/Fluids, **85**, 82–89, 2021, doi: 10.1016/j.euromechflu.2020.08.009.
40. K. HIEMENZ, *Die Grenzschicht an einem in den gleichförmigen Flüssigkeitsstrom eingetauchten geraden Kreiszyylinder [The boundary layer on a straight circular cylinder immersed in a uniform fluid stream]*, Dingler Polytechnisches Journal, **326**, 321–410, 1911.

Received June 9, 2024; revised version August 26, 2024.

Published online October 8, 2024.
